Master's Thesis
석사 학위논문

Structure and Electrochemical Properties of Magnesium Ion Intercalation into Vanadium Dioxide

Dedy Setiawan

Department of
Energy Science & Engineering

DGIST

2020

Structure and Electrochemical Properties of Magnesium Ion Intercalation into Vanadium Dioxide

Advisor: Professor Seung-Tae Hong
Co-advisor: Professor Hochun Lee

By

Dedy Setiawan
Department of Energy Science & Engineering
DGIST

A thesis submitted to the faculty of DGIST in partial fulfillment of the requirements for the degree of Master of Science in the Department of Energy Science & Engineering. The study was conducted in accordance with Code of Research Ethics[1)].

11. 20. 2019

Approved by

Professor Seung-Tae Hong (signature)
(Advisor)

Professor Hochun Lee (signature)
(Co-Advisor)

1) Declaration of Ethical Conduct in Research: I, as a graduate student of DGIST, hereby declare that I have not committed any acts that may damage the credibility of my research. These include, but are not limited to: falsification, thesis written by someone else, distortion of research findings or plagiarism. I affirm that my thesis contains honest conclusions based on my own careful research under the guidance of my thesis advisor.

Structure and Electrochemical Properties of Magnesium Ion Intercalation into Vanadium Dioxide

Dedy Setiawan

Accepted in partial fulfillment of the requirements for the degree of Master of Science.

11. 20. 2019

Head of Committee _____ (signature)
Prof. Seung-Tae Hong

Committee Member _____ (signature)
Prof. Hochun Lee

Committee Member _____ (signature)
Prof. Yong Min Lee

MS/ES
201824002

Dedy Setiawan. Structure and Electrochemical Properties of Magnesium Ion Intercalation into Vanadium Dioxide. Department of Energy Science & Engineering. 2020. 40p. Advisors Prof. Seung-Tae Hong, Co-Advisors Prof. Hochun Lee.

Abstract

Magnesium-ion Batteries (MIBs) offer a promising energy density, safety, and low-cost energy storage due to the large abundance of magnesium on Earth. However, only limited candidates have been proposed for MIBs cathode materials. In this study, the structure and electrochemical properties of magnesium ion intercalation into vanadium dioxide (VO_2(B)) has been unveiled. VO_2(B) was synthesized using a facile hydrothermal method, and confirmed by XRD, HR FE-SEM and TEM as a monoclinic structure with the space group of *C 2/m*, and a nano-belt morphology. The material shows reversible magnesium intercalation with a discharge capacity of 51.0 mAh g^{-1} at 25^{o}C at current density of 20 mA g^{-1} in nonaqueous electrolyte (0.5 M $Mg(ClO_4)_2$ in AN). It shows good rate performance at 25, 30, 40, and 50 mA g^{-1}. The cycle performance of VO_2(B) still need improvement, as it delivered 62% of the initial capacity after 25 cycles, due to the structural degradation and vanadium dissolution in the electrolyte.

VO_2(B) also shows magnesium intercalation with a discharge capacity of 114.8 mAh g^{-1} with an average voltage of ~2.47 V (vs Mg/Mg^{2+}) at 60^{o}C in nonaqueous electrolyte. The structural evolution at pristine, discharge, and charge state revealed the magnesium ion intercalation into VO_2(B). The crystal structure of $Mg_{0.11}VO_2$ and detail magnesium ion position in VO_2(B) is determined for the first time. It has monoclinic structure with space group of *C 2/m* and the magnesium ion is located in the largest cavity of VO_2(B). TEM-EDX mapping and XPS result also revealed the reversible magnesium intercalation into the material.

Keywords: Magnesium ion battery, Structure, Electrochemical properties, Vanadium dioxide, Nonaqueous electrolyte

List of Contents

List of Figures

List of Tables

I. INTRODUCTION

1.1. Rechargeable Batteries

The drastic growing of energy needs from modern industry have been pushing important works in generating high performance and efficiency energy storages. Rechargeable batteries, especially lithium ion battery technology, has so far provided answer for the current demand. As shown in Fig. 1., gravimetric and volumetric energy density of lithium ion battery which is the highest among other types of battery is also one of the consideration. Since its commercialization in 1991, modern lithium ion batteries has reach ten times cheaper prize, due to its large production, and distribution among all daily life technologies. However, the demanding of more energy density has kept the researches in enormous number. [1-3]

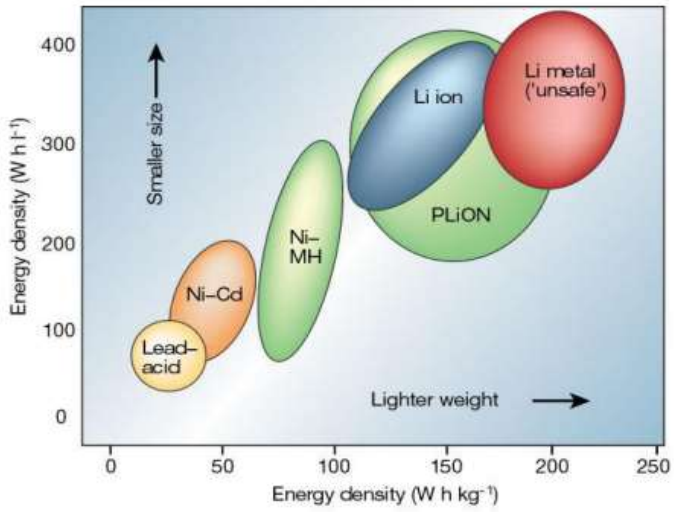

Figure 1. Gravimetric and volumetric energy density of batteries [3]

The principle of rechargeable batteries, in this case lithium ion batteries, involves a positive (cathode) and negative (anode) electrodes, and electrolyte which transports the lithium ions during charge and discharge process. In 1972, TiS_2 was applied as intercalation cathode material, lithium perchlorate in dioxolane as the electrolyte, and lithium metal as the anode by

Exxon. Later on, lithium metal oxides, including lithium cobalt oxide, with layered structure was proposed by Goodenough, which commercialized as current lithium ion batteries. However, the safety concern of lithium metal anode in terms of dendrite growing has driven into graphite as commercial anode material in lithium ion batteries system. To date, the remaining challenge of existing rechargeable batteries lies on the design and combination of electrode materials, as well as electrolyte, which can provide much better life cycle and demanding energy density. [4,5]

1.2. Multivalent ion Batteries

Energy storage technologies such as lithium-ion batteries (LIBs) have enabled the development of ubiquitous portable electronic devices including mobile, laptop, electric vehicles, and energy storage systems. Since the pioneering commercialization by Sony Corporation in 1991 with high voltage and energy cell, rechargeable LIBs has so far offered astonishing prospect as the modern one exhibits more than twice in case of energy per weight. [1,2] Despite, the concerns of limiting lithium distributions in the world, cell engineering, and processing cost are in the list of challenges which must be tackled in perspective of many researchers. [2,5] As one type of post-LIBs technology, the multivalent-ions batteries (including Mg^{2+}, Ca^{2+}, and Zn^{2+}) have been considered as having such properties which meet the criteria. [7-10]

As lithium ion battery system, multivalent ion batteries are expected to convert chemical energy by the component of a cathode, an anode, and an electrolyte which transports ions. The intercalation of 2+ cation allows high possibility of achieving higher capacity compared to current lithium ion battery system. Using metallic anode, multivalent ion batteries also offer promising energy density improvement (3833 mAh cm^{-3} for magnesium metal) compared to lithium ion batteries (~2046 mAh cm^{-3} for lithium metal). Furthermore, lithium metal hasn't considered good enough for commercial use due to growing of surface reaction with electrolyte

which cause lack of long cycle performance and safety. Even it is normally used for laboratory characterization, the commercial lithium ion battery still put its trust on graphite anodes (~800 mAh cm^{-3}). In this point of view, several developments of nonaqueous multivalent ion battery system has been undergoing, including its electrolyte, and especially its cathode material candidates. [7]

The research on multivalent ion batteries cathode material offers discovery of new materials and electrochemical intercalation chemistry. Although, the intercalation process may occurs sluggishly into oxide materials, due to strong Coloumbic interaction between cation and oxygen ions in the lattice structure. As a result, the electrochemical intercalation chemistry of multivalent ions into cathode materials are still considered as puzzling phenomena, as well as discovery of the functioning materials.

1.3. Magnesium Ion Battery

Among multivalent-ions based batteries candidate, magnesium-ion batteries (MIBs) have been explored through many types of research as it offers promising efficiencies, particularly in case of magnesium abundance on Earth's crust (29,000 ppm) compared to lithium (only 17 ppm). [8] The mechanism of magnesium ion batteries system is almost similar to lithium ion batteries. The researches mainly focus on discovering intercalation mechanism electrode materials and electrolytes which facilitate magnesium-ions to transport between the cathode and anode. However, only limiting materials have been discovered as the cathode candidate for MIBs. Several reports include the pioneering magnesium battery prototype using Chevrel phase $Mg_xMo_3S_4$ cathode material with less than 15% capacity fading, published by Prof. Aurbach and group in 2000. [11] Intercalation mechanism of magnesium ions on the Chevrel phase was also investigated by later reports. [12-15] Besides, other types of material such as Oxides and Polyanions also have been recently studied. [16-24]

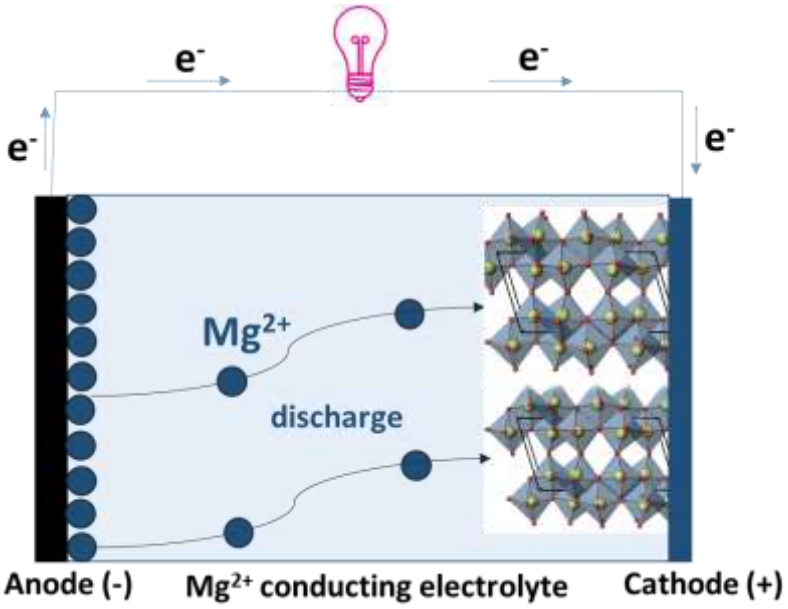

Figure 2. The working principle of magnesium ion battery

The possibility of achieving higher operating voltage is by applying oxygen as anion species, or more familiarly called as oxide materials. Several studies have been done by employing layered α-MoO_3, which offers high theoretical capacity of ~372.3 mAh g^{-1} for 2 electrons transfer. However, the ambiguous influence of electrolyte during cycling was noticed as reported by some papers. The studies on magnesium intercalation into α-V_2O_5 also have been reported. Besides, magnesium-ion intercalation into this structure is relatively sluggish in room temperature. Some efforts including higher temperature measurement or applying wet electrolyte has also been studied. [7-8]

The research on magnesium ion battery anode has focused on finding compatible metal or insertion material for conventional battery electrolyte. The reason behind this is the formation of blocking layer in the surface of magnesium metal anode while interact with conventional electrolyte. As a result, reversible magnesium ion diffusion seems challenging. Several reports include the possible magnesium insertion into Bi, Sb, and the combination of both insertion metal, Bi_xSb_y. Since the successful replacement of lithium metal into graphite, the similar technique may be applied for magnesium metal. [8]

The studies on electrolyte is going on the suitability with magnesium metal by electrodeposition. Earlier reports include possible magnesium ion insertion into host material using ionic salt, $Mg(BF_4)_2$ and $Mg(ClO_4)_2$ in conventional solvent. However, the passivation nature was observed when employing the electrolyte in magnesium metal. The magnesium insertions into host materials also exhibited in some organoborates including magnesium tributylphenyl $Mg(BPhBu_3)_2$) electrolyte. However, the electrolyte still suffered from oxidative stability. [8]

1.4. Vanadium Dioxides

Vanadium dioxide polymorphs exist in several crystal phases: VO_2(B), VO_2(A), VO_2(M), VO_2(R), and VO_2(C), where VO_2(B) and VO_2(A) are considered as metastable phases. [25] VO_2(B) is the brookite phase of vanadium dioxide which considered as the most stable open framework phase of the material. [33] As shown in Figure 3, the crystal structure of VO_2(B) has a monoclinic structure with space group of *C 2/m* and is formed by corners and edge-sharing between VO_6 octahedra, provides three diffusion cavities denoted as C_1, C_2, and C_3, and two diffusion paths along *b* and *c*-axis. Meanwhile, VO_2(A) crystal structure is reported to have low temperature phase and high temperature phase structure. Popuri et. al., suggested that the low temperature phase has tetragonal structure with space group of *P 4/ncc*, and is formed by four units of two edge-sharing VO_6 octahedra. The schematic drawing of VO_2(A) is shown in Figure 4.

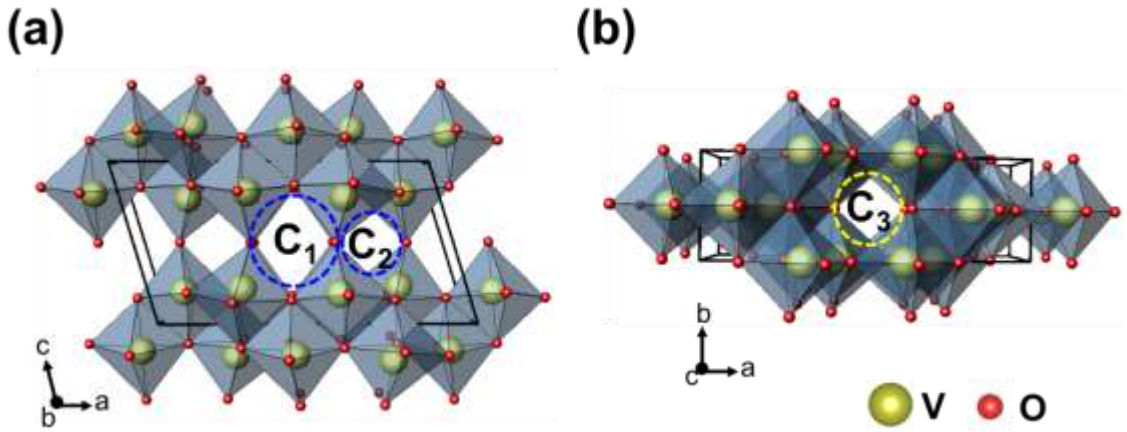

Figure 3. Crystal structure of VO_2(B) **(a)** a-c plane. **(b)** a-b plane.

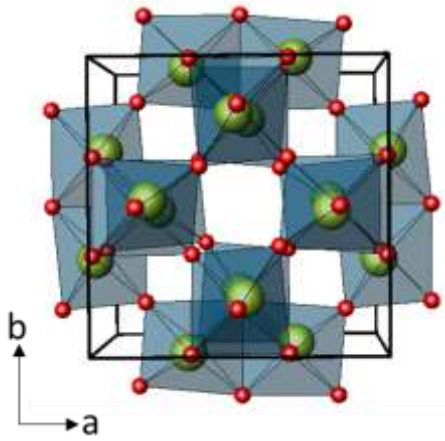

Figure 4. Crystal structure of VO_2(A)

Among all the phases of vanadium dioxides, VO_2(B) have been investigated as cathode material for Li, Na, K, and Zn-ion batteries intensively due to its structure and high theoretical capacity of 323.10 mAh g^{-1} per 1 electron.[25-40] In the recent study by Luo et. al., VO_2(B) exhibited an initial discharge capacity of 394 mAh g^{-1} at 12^0C. $Mg(ClO_4)_2$ in acetonitrile (AN) was utilized as an electrolyte. However, the water content in the electrolyte was not specifically mentioned, which limited a deep investigation of proton co-intercalation into the structure. [37] Moreover, electrochemical intercalation mechanism of magnesium-ions into the host structure is more considered as puzzling phenomena until now. Some reports also include VO_2(A) as

cathode material for lithium ion battery. However, most studies are still focusing on the synthesis process and the structure of the material.

In this work, VO_2(B) was investigated as a cathode material for MIBs using a nonaqueous electrolyte. We explored the electrochemical performance through galvanostatic discharge-charge and cyclic voltammetry measurements. The evidence of magnesiation was conducted by X-ray diffraction, elemental analyses, transmission electron microscopy, and X-ray photoelectron spectroscopy. Fourier electron density analysis was used to determine the magnesium position in the VO_2(B) structure.

1.5. Research Objectives

This research has several objectives, including to study the structure of vanadium dioxide (VO_2(B)), to investigate the electrochemical properties of magnesium ion intercalation into vanadium dioxide (VO_2(B)) in nonaqueous electrolyte, to analyze the intercalation mechanism and to determine the structure of magnesium intercalated vanadium dioxide (Mg_xVO_2(B)).

II. METHODS

2.1. Synthesis

VO_2(B) powder was prepared via a facile hydrothermal method by mixing V_2O_5 (99.8%, Alfa Aesar) and oxalic acid (98%, Sigma Aldrich) as reduction agent with a molar ratio of 1: 2.4 in 50 ml of D.I. water. The mixture was continuously stirred at 40 ^{0}C for 22 h until the light blue color was identified. The solution was then transferred into 100 ml Teflon lined stainless-steel autoclave, tightly closed and heated at 180 ^{0}C for 24 h. The resulting solution was filtered and washed with ethanol three times. Finally, the product was dried at 60^{0}C in vacuum for 6 h.

2.2. Material Characterization

The crystal structure of VO_2(B) was characterized using X-ray diffractometer (XRD, Rigaku Mini-Flex 600) with Cu Kα radiation, λ = 1.5418 Å, and angle range between 10^o until 80^o with continuous scanning and scan rate of 1.5^o /min. The morphology of as-prepared powder was analyzed by high-resolution field emission scanning electron microscopy (HR FE-SEM, Hitachi SU-8020) and a high-resolution field-emission transmission electron microscopy (HR FE-TEM, Hitachi SU-8020, Japan) with an energy dispersive X-ray spectroscopy (EDX) was used to qualitatively determine the elemental composition. Induced coupled plasma optical emission spectroscopy (ICP-OES, Varian 700-ES) was used to quantitate magnesium amount for the discharged and charged electrode. The oxidation states of vanadium were determined using X-ray photoelectron spectroscopy (XPS, Thermo Scientific ESCALAB 250Xi) with Al Kα radiation.

2.3. Electrode, Electrolyte, and Cell Preparation

The electrodes were prepared by mixing active material (VO_2(B)) with conductive carbon (Super P carbon, Timcal Graphite & Carbon) and poly(vinylidene fluoride) (PVDF) binder (W#1300, Kureha Co.) with the weight ratio of 8: 1: 1 in *N*-methyl-2-pyrrolidone (NMP). The mixture was coated on carbon-coated stainless steel foil (SUS-304L) with the thickness of 40 μm and dried at 60 ^{0}C in vacuum for 6 h. The coating resultants were pressed and cut into a circle shape with an area of 1.53 cm^2 to make electrodes. The average loading mass of electrode was noticed as ~3.0 mg.

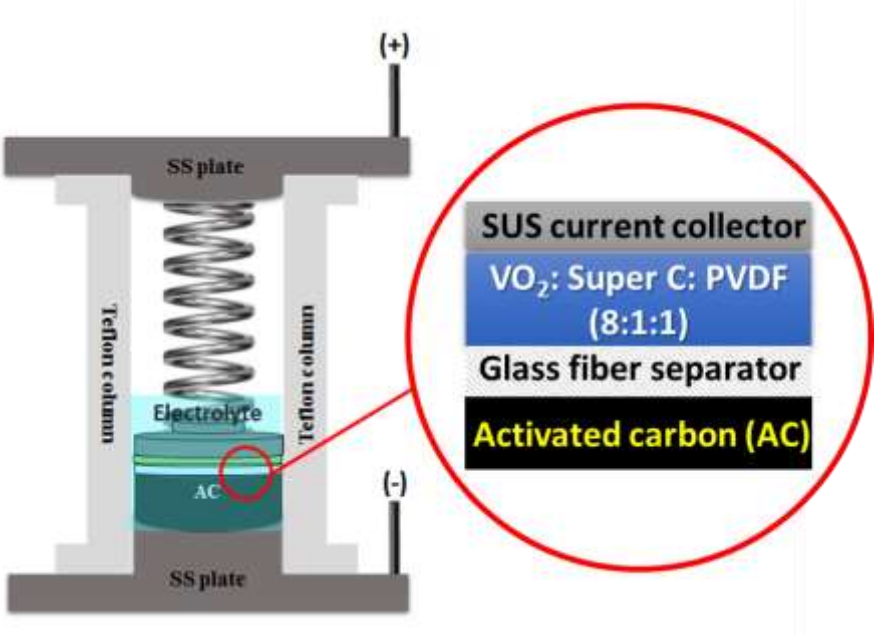

Figure 5. Schematic drawing of homemade cell for electrochemical measurement

Homemade cell (Fig. 5.) was assembled with VO_2(B) as working electrode, 0.8 g of activated carbon pellet (Daejung Chemicals) as a counter electrode. A glass fiber (GF/A, Whatman) was used as a separator, after fully dried at 120^{0}C for 3 days and 0.5 M of $Mg(ClO_4)_2$ (ACS reagent grade, Alfa Aesar) in acetonitrile (99.8%, Samchun, Korea) were utilized as an electrolyte. The water content of the electrolyte was 40 ppm, measured using Karl Fischer coulometer (Metrohm, 831 KF coulometer). The $Mg(ClO_4)_2$ was dried at 220^{0}C for 24 h, and the Acetonitryl was treated with molecular sieves. Additionally, all electrochemical cell

components were dried at 80 ^{0}C before assembling the cell to avoid the dramatic increase of water content during electrochemical measurements.

2.4. Electrochemical Characterization

EC-lab software on a Biologic VMP3 multichannel potentiostat (Biologic Science Instruments SAS) was used to measure galvanostatic discharge-charge and Cyclic Voltammetry (CV). A constant voltage was applied during the charging process to maximize the extraction of magnesium-ions until the current dropped to 20% of the current density.

2.5. Structural Analysis

The pristine, discharged and charged electrodes crystal structure were characterized using a PANalytical Empyrean X-ray diffractometer was used with a copper Kα_1 X-ray (λ = 1.5406 Å) with a primary germanium (111) monochromator, a position-sensitive PIXcel3D 2×2 detector, with a total measurement time of 12 h at room temperature. Rietveld refinement of the pristine material and the discharge electrode were performed using the powder profile refinement program, *GSAS*. [46] The crystal structure of discharge electrode was determined using a combination of the powder profile refinement program, *GSAS.* and the single-crystal structure refinement program, CRYSTALS, as described in our previous work. [47,48] MCE was used to obtain a three-dimensional (3D) view of the Fourier density maps. [49]

III. RESULT AND DISCUSSION

3.1. Structure and Morphology

The VO_2(B) powder was successfully synthesized using a facile hydrothermal method, with oxalic acid as a reduction agent. The Rietveld refinement result of as-prepared powder XRD data presented in Fig. 6. suggests a monoclinic crystal structure with a space group of *C 2/m* and cell parameters of a = 12.059 (1) Å, b = 3.692 (2) Å, c = 6.420 (1) Å. No impurity was evolved, which means V^{5+} was successfully reduced into V^{4+} during the synthesis process. The information of refined atomic parameters and interatomic distances are provided in Table 1 and 2.

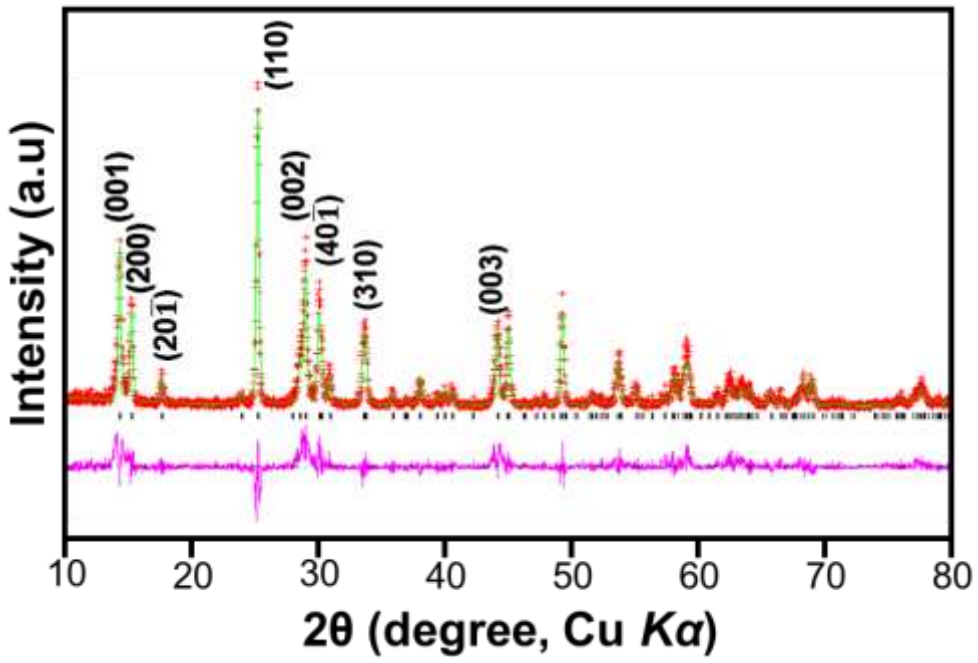

Figure 6. The Rietveld refinement result of VO_2(B) powder

Table 1. Crystallographic data and powder XRD Rietveld refinement results for VO_2(B): atomic coordinates, site occupancies, isotropic displacement parameters, and reliability factors.

Crystal System	Monoclinic
Space Group	C 2/m
Lattice Parameter, Volume, Z	a = 12.059 (1) Å, b = 3.692 (2) Å, c = 6.420 (1) Å, V = 273.42 (3) Å^3, $\alpha = \gamma = 90^o$, $\beta = 106.96\ (1)^o$ Z = 4

Atoms	x	y	z	Wyckoff	Occupancy	$U_{iso} \times 100$
V1	0.6006 (3)	0.0000	0.1852 (4)	4c	1	1.7
V2	0.3011 (3)	0.0000	0.2211 (4)	4c	1	1.7
O1	0.1213 (3)	0.0000	0.1925 (4)	4c	1	1.7
O2	0.4433 (3)	0.0000	0.1493 (4)	4c	1	1.7
O3	0.7663 (3)	0.0000	0.1561 (4)	4c	1	1.7
O4	0.3602 (3)	0.0000	0.5003 (4)	4c	1	1.7

** $R_p = 0.236$, $R_{wp} = 0.341$, Rexp = 0.259, $R(F^2) = 0.169$, $\chi^2 = 1.769$*

Table 2. Selected interatomic distances (Å) in the structure of VO_2(B).

V1–O1	1.8616 (1) Å × 2	**V2–O1**	2.1219 (2) Å
V1–O2	1.8428 (1) Å 2.0570 (5) Å	**V2–O2**	1.9010 (1) Å
V1–O3	2.0604 (2) Å	**V2–O3**	1.9121 (1) Å × 2 2.3190 (5) Å
V1-O4	1.9340 (5) Å	**V2–O4**	1.7251 (2) Å

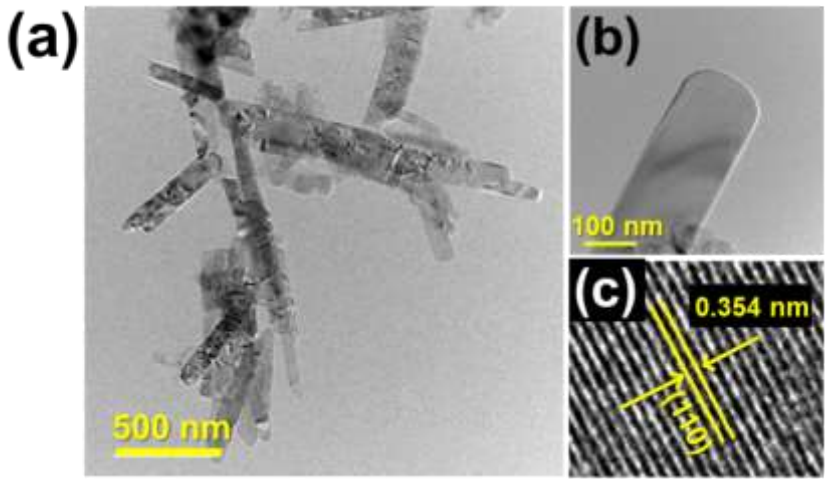

Figure 7. TEM images with a different magnification **(a)** 500 nm **(b)** 100 nm, and **(c)** HR-TEM image with (110) fringes.

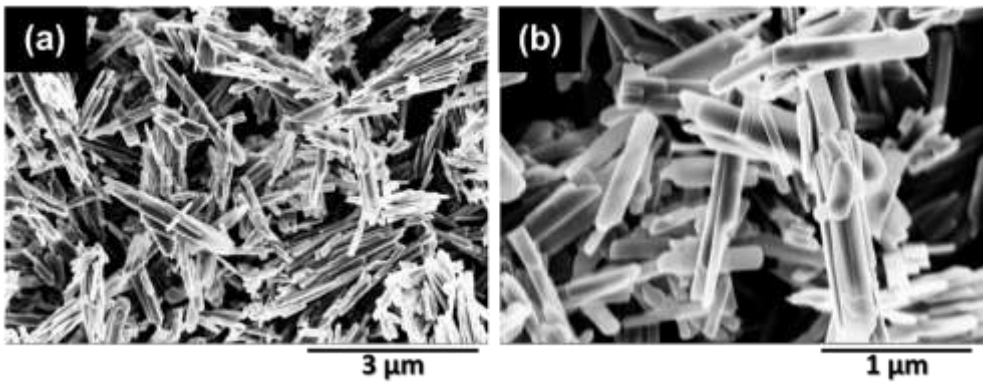

Figure 8. SEM images with a different magnification **(a)** 3 µm **(b)** 1µm.

Fig.7. a and b show the TEM images of VO_2(B) powder in different magnifications which can be seen as the nano-belt shape with a width of ~200 nm. The interplanar distance of 0.35 nm in Fig. 7.c. can be indexed to $d_{(110)}$ spacing of VO_2(B). Fig. 8. a. and b. show the SEM images of nanobelt morphology which consistent to the previous TEM images.

3.2. Electrochemical Properties

3.2.1. Wet vs. Dry Electrolyte

Firstly, the electrochemical behavior of VO_2(B) was investigated at two different water contents of the electrolyte condition, dry (40 ppm) and wet (650 ppm) at room temperature. Fig. 9. a. depicts the CV profile in wet electrolyte with a scan rate of 0.1 mV s^{-1} figuring sharper reduction peak at -0.57 V vs AC, compared to in dry electrolyte. Meanwhile, the oxidation peak in dry electrolyte is appeared at a higher voltage (0.35 V vs AC) compared to in wet electrolyte (0.18 V vs AC). Interestingly, two peaks are observed in wet electrolyte at the voltage of 0.18 and 0.40 V vs AC, which probably due to complex redox reaction from the protons or hydronium ions intercalation reaction as well as magnesium ions.

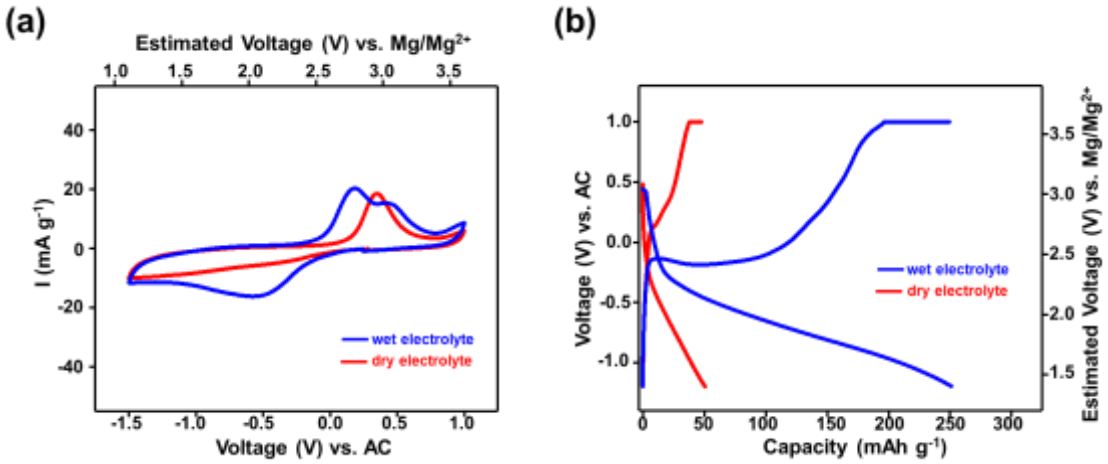

Figure 9. (a) CV profile of VO_2(B) in dry electrolyte (39 ppm) and wet electrolyte (650 ppm) at 25 ^oC (b) The galvanostatic discharge-charge of VO_2(B) in dried and wet condition at 25 ^oC with a current density of 20 mA g^{-1}.

As shown in Fig. 9. b. the galvanostatic discharge-charge was applied at 1.0 and -1.2 V vs AC with a current density of 20 mA g^{-1} in both electrolyte condition. VO_2(B) exhibited much

larger discharge and charge capacity of 250 mAh g^{-1} in wet electrolyte compared to dried electrolyte (51 mAh g^{-1}). Nevertheless, the registered discharge-charge capacity is still lower than previously reported by Luo et. al. [37] Therefore, it is reasonable to conclude that the drastic increase of specific capacity and sharper CV reduction peak was probably stimulated by proton co-intercalation rather than only magnesium-ion intercalation, forming $Mg_xH_yVO_2$ discharge product. [51] The XRD profile after discharge in wet electrolyte is shown in Fig. 10. In order to confirm the proton or hydronium ions intercalation, ICP (Table 3) and TEM-EDX mapping (Fig. 11.) were applied for after discharge in the wet electrolyte, observing a very small amount of magnesium, and not match with the correspondence discharge capacity.

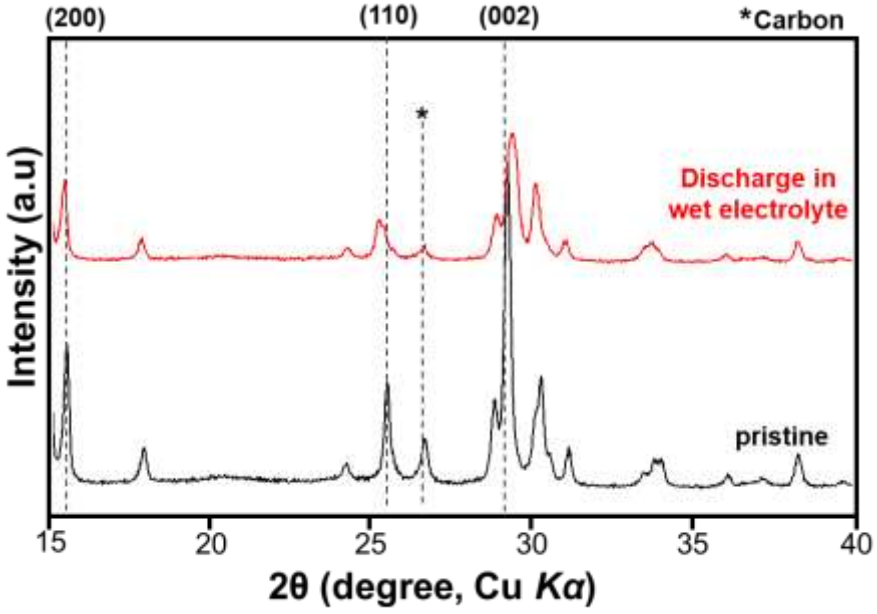

Figure 10. XRD after discharge in wet electrolyte

Table 3. Elemental ratios estimated from the ICP-OES analysis for the discharged electrode in the wet organic electrolyte (water contents of the electrolyte is 650 ppm).

Sample	Mass Ratio (%)		**Relative Atomic Ratio**	
	Mg	V	**Mg**	**V**
Discharged	2.25	97.7	**0.05**	**1.000**

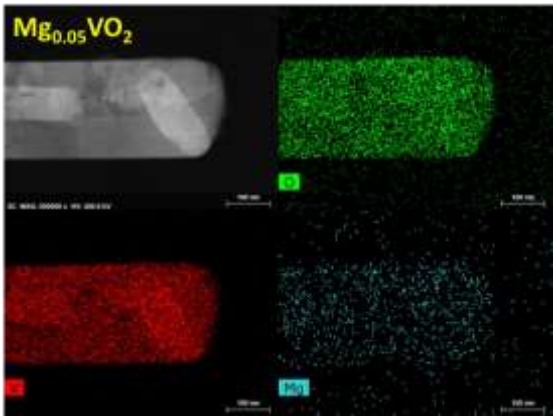

Figure 11. TEM-EDX mapping of discharge electrode in wet electrolyte

3.2.2. Room Temperature

The CV profile of VO_2(B) at room temperature was measured at 0.1 mV s^{-1} at the voltage range of -1.5 V – 1.0 V vs. AC using the nonaqueous electrolyte, 0.5 $Mg(ClO_4)_2$ in AN (water content is 40 ppm). As shown in Fig. 12. The reduction peak appeared very broadly, suggesting a sluggish magnesium ions intercalation, and difficult V^{4+} reduction into V^{3+}. Morover, the existing broad peak in the first cycle continues at the following cycle. Meanwhile, the oxidation peak appeared sharply at 0.35 V vs AC, or estimated to be 2.96 V vs. Mg/Mg^{2+}. The oxidation peak position doesn't change at the following cycle, suggesting a stable oxidation processes. The current at the 2nd cycle is found to be higher than the 1st cycle, suggesting the activation process of the material.

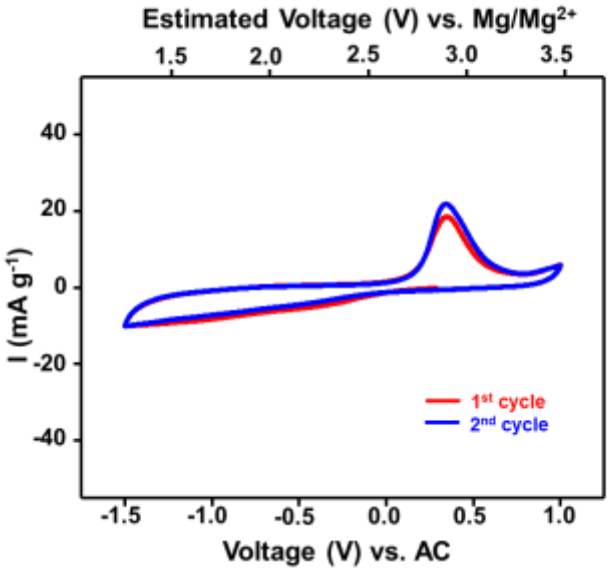

Figure 12. CV 1st and 2nd cycle at room temperature with scan rate of 0.1 mV s^{-1}

The galvanostatic discharge-charge at voltage range of -1.2 V – 1.0 V vs AC with a current density of 20 mA g^{-1} (Fig 13.) shows the material delivered discharge capacity of 51 mAh g^{-1}. According to the theoretical capacity of ~323.10 mAh g^{-1}, the delivered discharge capacity correspond to 0.16 electrons transfer or 0.08 magnesium ions intercalation. Therefore, the discharge electrode is estimated to have a formula of $Mg_{0.08}VO_2$. At the same current density, the material delivered reversible charge capacity of 48 mAh g^{-1}, correspond to 0.15 electrons or 0.07 magnesium ions were extracted from the host material. Additionally, the material shows higher and reversible capacity of 57 mAh g^{-1} after the 2nd cycle.

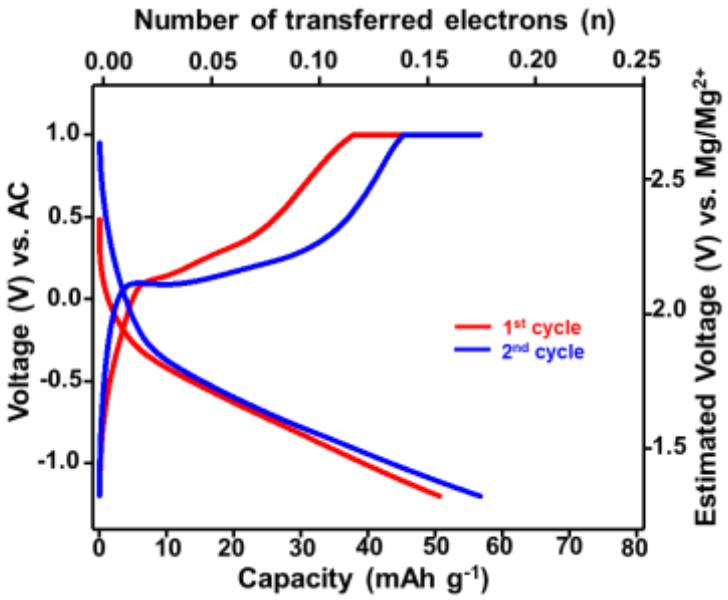

Figure 13. The galvanostatic discharge-charge at voltage range of -1.2 V – 1.0 V vs AC with a current density of 20 mA g^{-1} at room temperature

The cycle performance of VO_2(B) with current density of 20 mA g^{-1} at room temperature is shown in Fig. 14.a. The discharge capacity is 35 mAh g^{-1} (62 % of the 2nd cycle capacity) after 25 cycles. The capacity loss probably corresponds to structural degradation of VO_2(B) after cycles (Fig. 15) and vanadium dissolvation in the electrolyte, as 2 ppm Vanadium is noticed using ICP-OES. The rate performance of VO_2(B) is shown in Fig. 14. b. The material exhibit discharge capacity of 38, 33, 31, and 30 mAh g^{-1} at current density of 25, 30, 40, 50 mA g^{-1} respectively. The discharge capacity was recovered to 47 mAh g^{-1} after it was changed back to the initial current density (25 mA g^{-1}). The properties shows that VO_2(B) has good rate performance at room temperature in nonaqueous electrolyte.

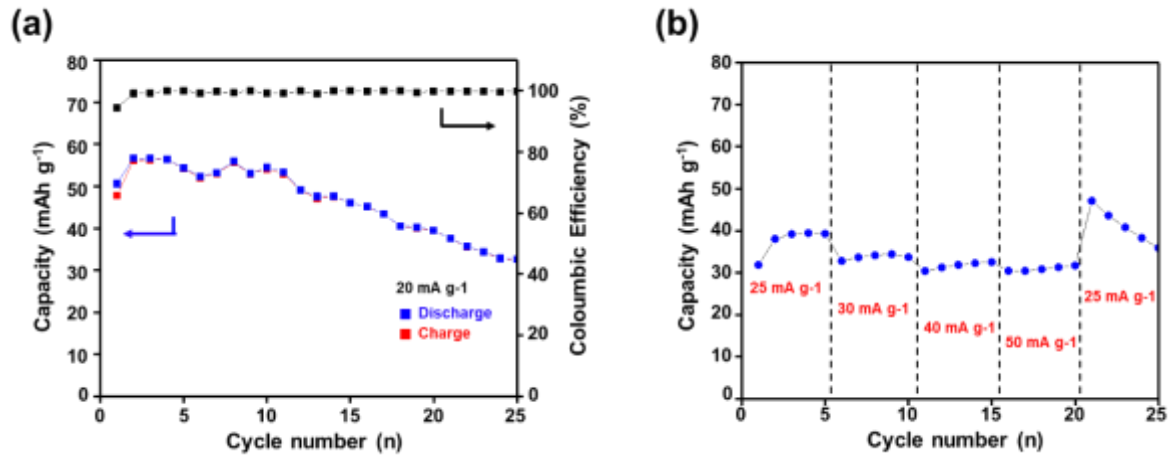

Figure 14. (a) The cycle performance of VO_2(B) at 25°C at current density of 20 mA g^{-1} (b) The rate performance of VO_2(B) at 25, 30, 40, and 50 mA g^{-1}

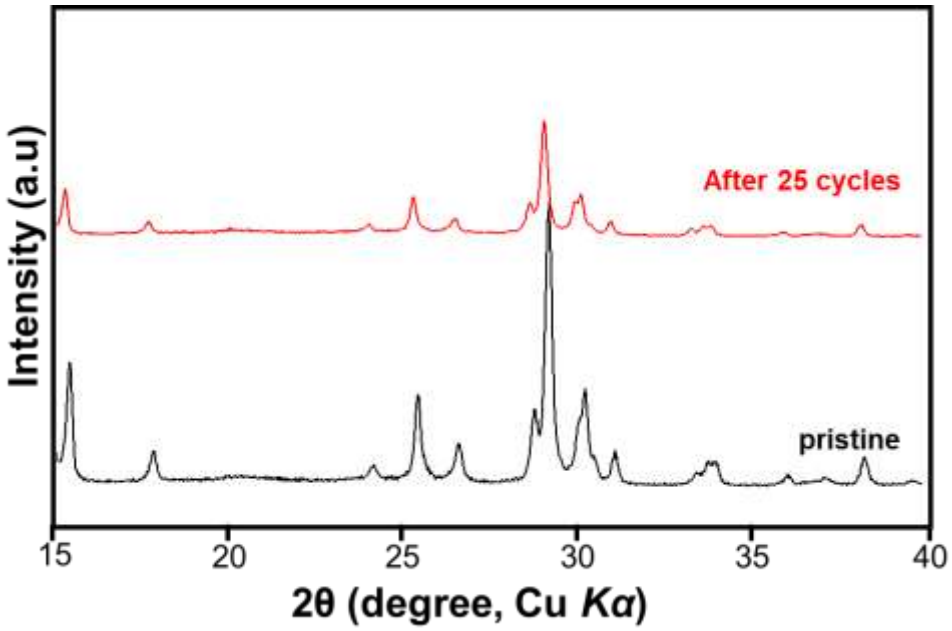

Figure 15. XRD profile of VO_2(B) after 25 cycles at 25°C

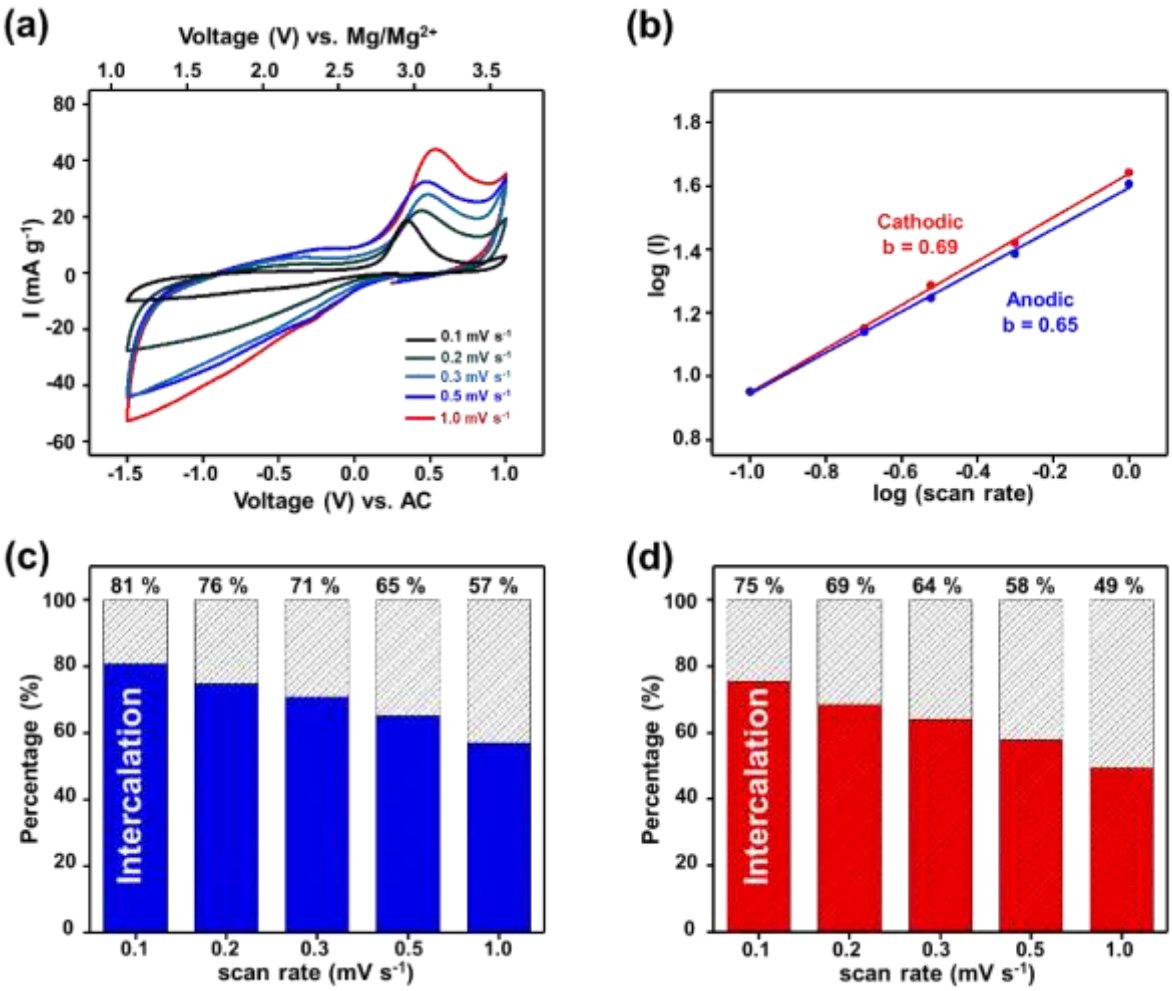

Figure 16. (a). The CV profile at scan rates of 0.1, 0.2, 0.3, 0.5, and 1.0 mV s^{-1} at room temperature. (b). log (I) vs log (scan rate) plot. (c) and (d). Capacitive and intercalation distribution in anodic and cathodic, respectively.

The CV measurement was further acquired at five different scan rates, 0.1, 0.2, 0.3, 0.5, and 1.0 mV s^{-1} to identify diffusion controlled and surface limited behavior in VO_2(B) structure. As shown in Fig. 16.a. the reduction peaks are observed broadly at all scan rate. Meanwhile at faster scan rate, the oxidation peaks are shifted toward higher voltage, corresponds to slower ionic diffusion. In order to elucidate the magnesium storage mechanism during CV measurement, the power-law relationship was calculated between *i* (current density) and *v* (scan rate), $i = av^b$, where *a* and *b* are constant. As the value of b is between 0.5 and 1, some of the electrochemical reaction is contributed by capacitive behavior (Fig. 16.b.). The

quantification of the intercalation and capacitive contribution was calculated using the equation of $i = k_1 v + k_2 v^{1/2}$, where k_1 and k_2 are the intercalation and capacitive contribution, respectively. [49] As shown in Fig. 16.c and d. the reduction and oxidation reaction is dominated by the intercalation mechanism, around 81-75% of magnesium ions are intercalated at a scan rate of 0.1 mV s^{-1}. As the increasing of scan rate to 1 mV s^{-1}, the surface-limited mechanism slowly increases. The results clearly demonstrate that the diffusion-controlled reaction is the mainly contribute to the magnesiation mechanism of VO_2(B).

3.2.3. Elevated Temperature

In order to gain more intercalated magnesium ions, the galvanostatic discharge-charge was also investigated at 60 °C (Fig. 17.). The discharge capacity at 20 mA g^{-1} was 115 mAh g^{-1}, corresponds to 0.35 electron transfer or ~0.17 magnesium ions intercalation. The increased specific capacity and number of magnesium ions intercalation at 60 ^{o}C compared to at 25 ^{o}C probably corresponds to the activation energy of VO_2(B) which has a relationship with the measurement temperature. However, at this measurement condition, the magnesium ions intercalation process seems to be not reversible, as the material only delivered charge capacity of 105 mAh g^{-1}, correspond to only 0.32 electrons transfer or 0.16 magnesium ion extraction. The rest of magnesium ions we expect to be stucked in the host material, due to difficult V^{3+} to V^{4+} oxidation process.

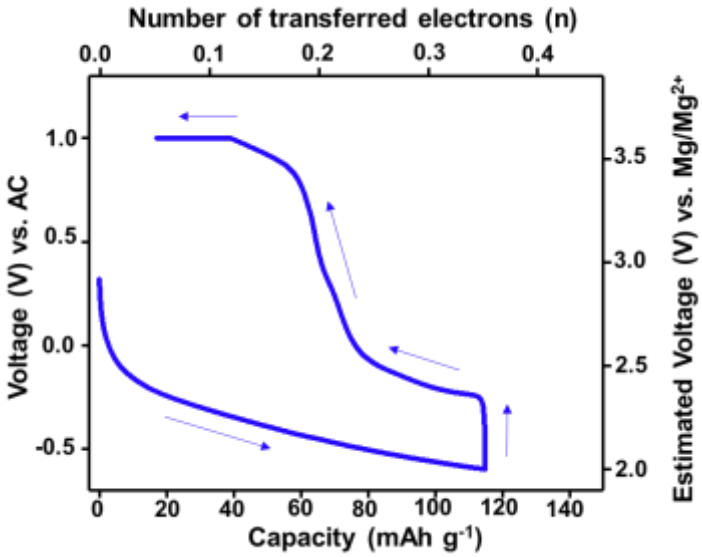

Figure 17. the galvanostatic discharge-charge investigated at 60 °C

The CV measurement was also acquired at five different scan rates, 0.1, 0.2, 0.3, 0.5, and 1.0 mV s^{-1} to identify diffusion controlled and surface limited behavior in VO_2(B) structure at 60ºC. The measurement was conducted with a voltage window between -0.6 V and 1.0 V vs AC at 60 ºC. As depicted in Fig. 18.a. the reduction peaks are observed slightly at ~0.37 V vs AC at all scan rates. The peaks indicate that the reduction process occurred more facile compared to at 25 ºC. The reason for the peak appearance may be related to the activation process at a higher temperature. Furthermore, the sharp oxidation peak appeared at -0.13 V vs AC with a scan rate of 0.1 mV s^{-1} and started shifting to a higher voltage in increasing scan rates. The voltage of reference electrode (AC) was estimated to be 2.61 V vs Mg/Mg^{2+} by comparing the redox peaks of CV profiles using the AC reference electrode with that obtained using a Ag/Ag^{+} reference electrode calibrated by the ferrocene/ferrocenium (Fc/Fc^{+}) redox couple (Fig. 19). The average redox peaks voltage of VO_2(B) was noted as ~2.47 V vs Mg/Mg^{2+}. As shown in Fig. 18 c. and d. the reduction and oxidation reaction is dominated by the intercalation mechanism, around 89-83% of magnesium ions are intercalated at a scan rate of 0.1 mV s^{-1}.

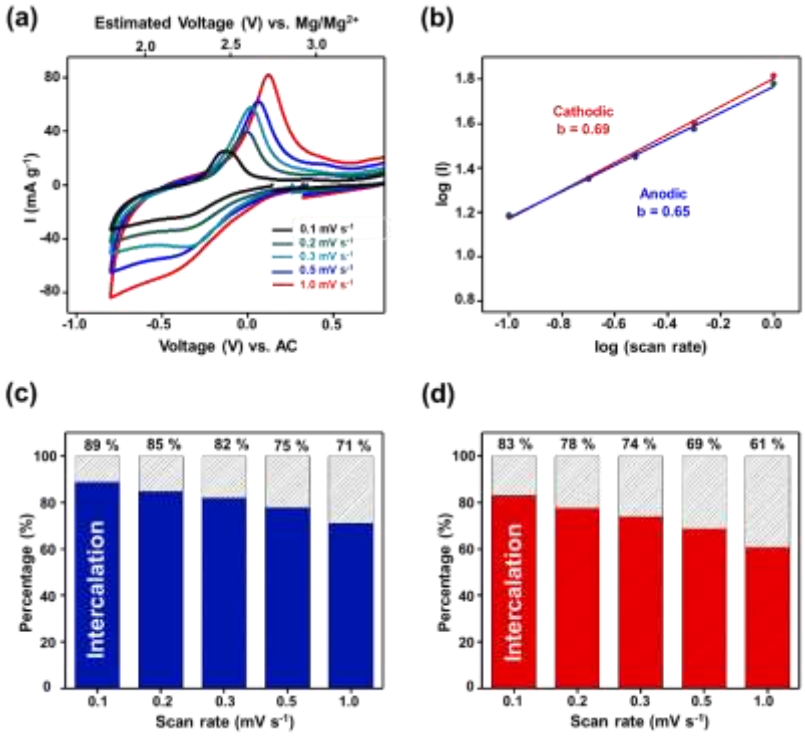

Figure 18. The CV profile at scan rates of 0.1, 0.2, 0.3, 0.5, and 1.0 mV s^{-1} at 60ºC. (b). log (I) vs log (scan rate) plot. (c) and (d). Capacitive and intercalation distribution in anodic and cathodic, respectively.

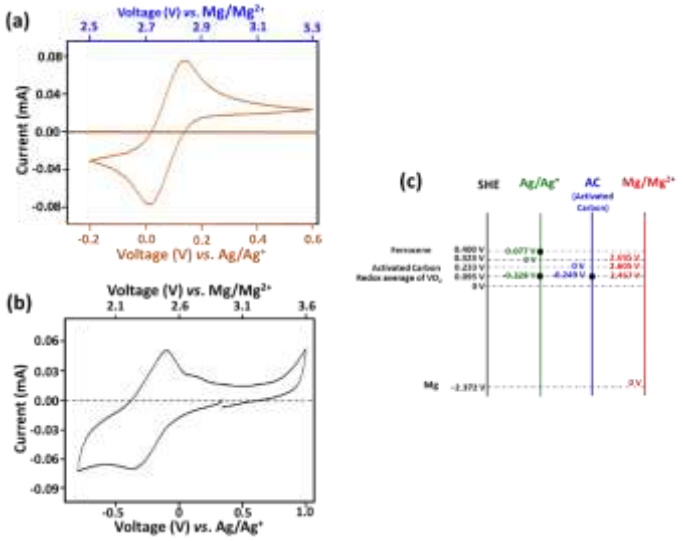

Figure 19. (a) The the ferrocene/ferrocenium (Fc/Fc^{+}) redox couple. **(b)** The CV profile of VO_2(B) vs Ag/Ag^{+}. **(c)** Estimated working voltage of VO_2(B)

3.3. Structural Analysis

The XRD profile of discharge electrode at 25°C is shown in Fig. 20. The peaks evolution is hardly observed, due to only small amount of magnesium ion was intercalated (0.08). Therefore, further structural analysis was conducted with the electrodes at 60°C measurement. The evolution of the XRD patterns of pristine, discharge and charge state at 60°C is shown in Fig. 21. The nano-belt morphology of VO_2(B) governed a preferred orientation in (00*l*) peaks, as pressure was applied during electrode preparation. In bigger magnification, (110) peaks shifted slightly into a lower angle during discharge, indicating the unit cell parameter *a* and b slightly increased by 12.059 to 12.067 Å and 3.692 to 3,709 Å at discharge state of -0.6 V, respectively. Upon the following charge, the peaks returned into initial position almost the same as the pristine. Interestingly, all (00*l*) peaks were slightly shifted to a higher angle, possibly corresponds to decreasing unit cell in *c*-axis.

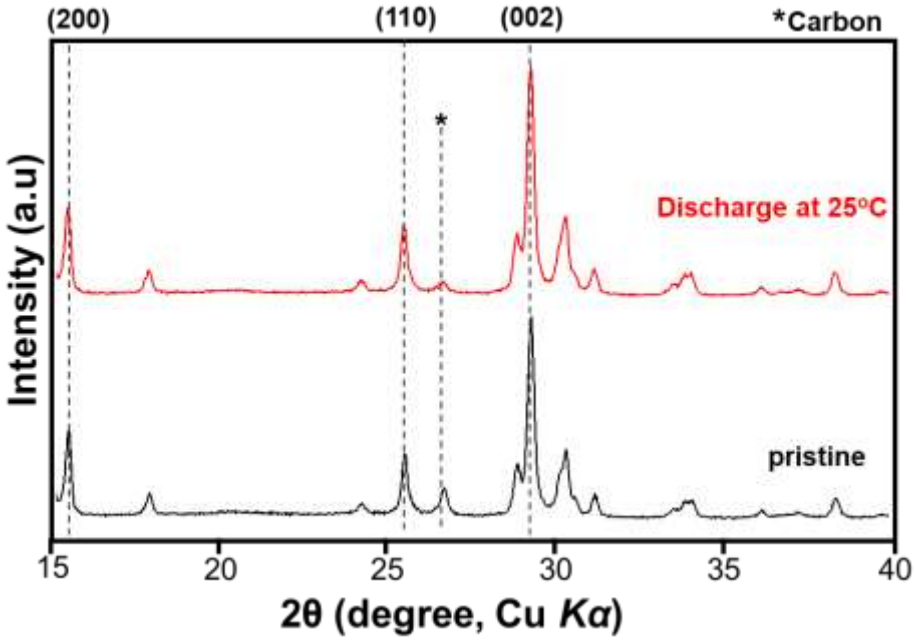

Figure 20. XRD profile of VO_2(B) at pristine and discharge at 25°C

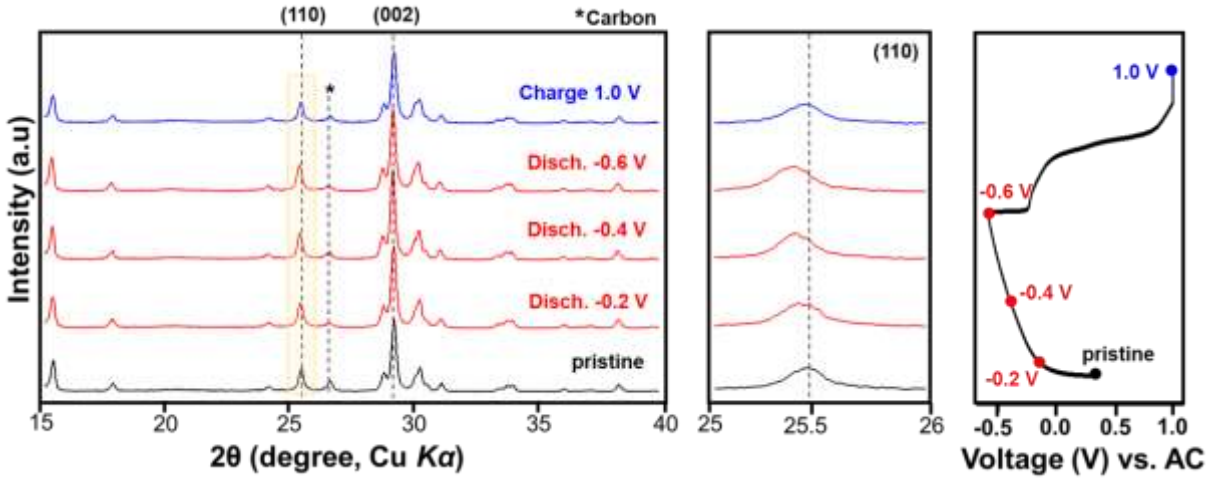

Figure 21. XRD profile evolution of VO_2(B) at pristine, discharge, and charge state. Carbon support is noted with (*).

Based on ICP-OES analysis, the discharge electrode has the amount of magnesium was 0.11 per unit formula, suggesting the chemical formula of $Mg_{0.11}VO_2$ (Table 4). This amount of magnesium is about 65% of that calculated from the discharge capacity (115 mAh g^{-1} at 20 mA g^{-1}, or $Mg_{0.16}VO_2$). Thus, it is suggested that rest of magnesium in the surface of VO_2 (B) was probably washed out during sample preparation, and also confirmed previously by electrochemical magnesium storage analysis that only ~83% of magnesium was perfectly intercalated.

Table 4. Elemental ratios calculated by ICP-OES analysis for pristine VO_2(B), discharge, and charge electrode.

Sample	Mass Ratio (%)		**Relative Atomic Ratio**	
	Mg	V	**Mg**	**V**
Pristine	N.D.	100	**0.00**	**1.00**
Discharge	4.85	92.1	**0.11**	**1.00**
Charge	1.12	98.4	**0.02**	**1.00**

The crystal structure of $Mg_{0.11}VO_2$ was determined and refined for the first time in this work, the magnesium position was solved by Fourier electron-density map from powder XRD

data using GSAS[38] and Crystals[39] as shown in Fig. 22. The Rietveld refinement of $Mg_{0.11}VO_2$ with the new magnesium position is presented in Fig. 23. It has the space group of *C2/m* with the unit cell of a = 12.067 (3) Å, b = 3.709 (2) Å, c = 6.416 (2) Å. The detail refined unit cell information and selected distances of $Mg_{0.11}VO_2$ are presented in Table 5 and 6, respectively.

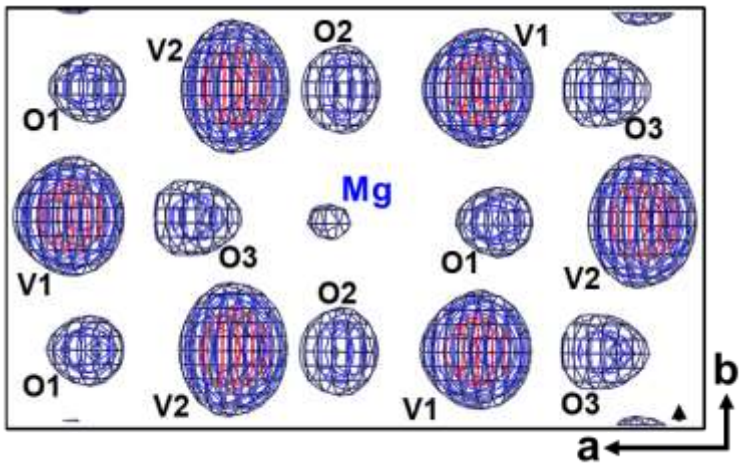

Figure 22. Electron density map of $Mg_{0.11}VO_2$

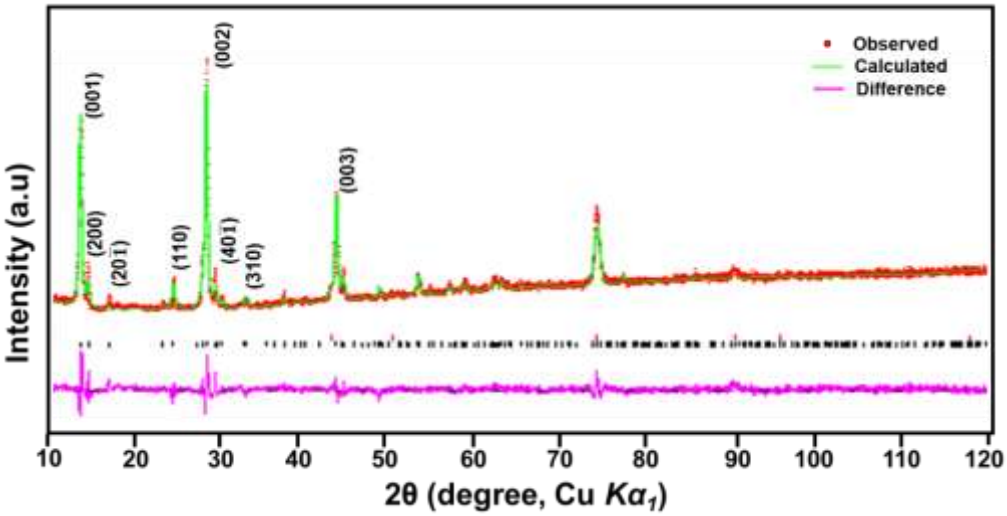

Figure 23. Rietveld refinement of $Mg_{0.11}VO_2$

Table 5. Crystallographic data and powder Rietveld refinement results for $Mg_{0.11}VO_2$: atomic coordinates, site occupancies, isotropic displacement parameters, and reliability factors.

Crystal System	Monoclinic
Space Group	C 2/m
Lattice Parameter, Volume, Z	a = 12.067 (3) Å, b = 3.709 (2) Å, c = 6.416 (2) Å, V = 274.66 (8) $Å^3$, $\alpha = \gamma = 90^0$, $\beta = 106.974\ (2)^0$ Z = 4

Atoms	x	y	z	Wyckoff	Occupancy	$U_{iso} \times 100$
V1	0.5978 (7)	0.0000	0.1887 (1)	4c	1	1.8
V2	0.2988 (6)	0.0000	0.2213 (2)	4c	1	1.8
O1	0.1190 (6)	0.0000	0.1924 (2)	4c	1	1.8
O2	0.4399 (7)	0.0000	0.1456 (1)	4c	1	1.8
O3	0.7629 (6)	0.0000	0.1568 (3)	4c	1	1.8
O4	0.3672 (1)	0.0000	0.4979 (7)	4c	1	1.8
Mg	0.5580 (8)	0.5000	0.7077 (3)	4c	0.22	1.8

* R_p = 0.059, R_{wp} = 0.083, R_{exp} = 0.045, $R(F^2)$ = 0.17943, χ^2 = 3.497

Table 6. Selected interatomic distances (Å) in the structure of discharged $Mg_{0.11}VO_2$.

V1–O1	1.8713 (6) Å x 2	**V2–O1**	2.1225 (3) Å
V1–O2	1.8448 (1) Å, 2.0584 (4) Å	**V2–O2**	1.9021 (3) Å
V1–O3	2.0612 (3) Å	**V2–O3**	1.9218 (6) Å x 2, 2.3205 (5) Å
V1-O4	1.9301 (4) Å	**V2–O4**	1.7251 (4) Å
Mg-O1	2.4020 (2) Å	**Mg-O3**	2.0800 (6) Å
Mg-O2	2.0760 (9) Å × 2	**Mg-O4**	2.5870 (2) Å × 2
Mg-Mg	2.6200 (4) Å		

The crystal structure of $Mg_{0.11}VO_2$ is shown in Fig 24.a. The magnesium-ions occupy the edge of the largest cavity in *b*-axis. Considering that non-bonded magnesium-oxygen is 2.59 Å, magnesium atom has 6-oxygen coordination in total, where 4 nearest oxygen coordination

(O1, O2, and O3) have the interatomic distance of 2.40, 2.08, and 2.08 Å, respectively (Fig.24.b.). Meanwhile, the other 2-oxygen coordination is considered as weak bonding (Mg-O4) with the interatomic distance of 2.58 Å.

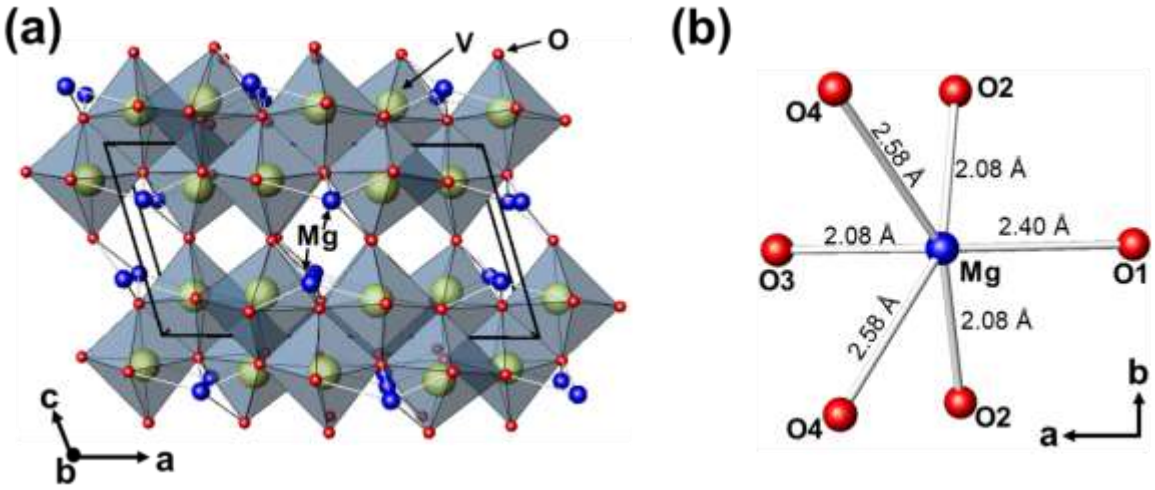

Figure 24. (a) The crystal structure of $Mg_{0.11}VO_2$. (b) Magnesium position at ab plane.

3.4. Elemental Analysis

The TEM-EDX mapping of pristine, discharge, and charge electrode shows in Fig. 25. A homogeneous distribution can be clearly seen in discharge electrode, which is vanished in the charge electrode, corresponding the reversible reaction.

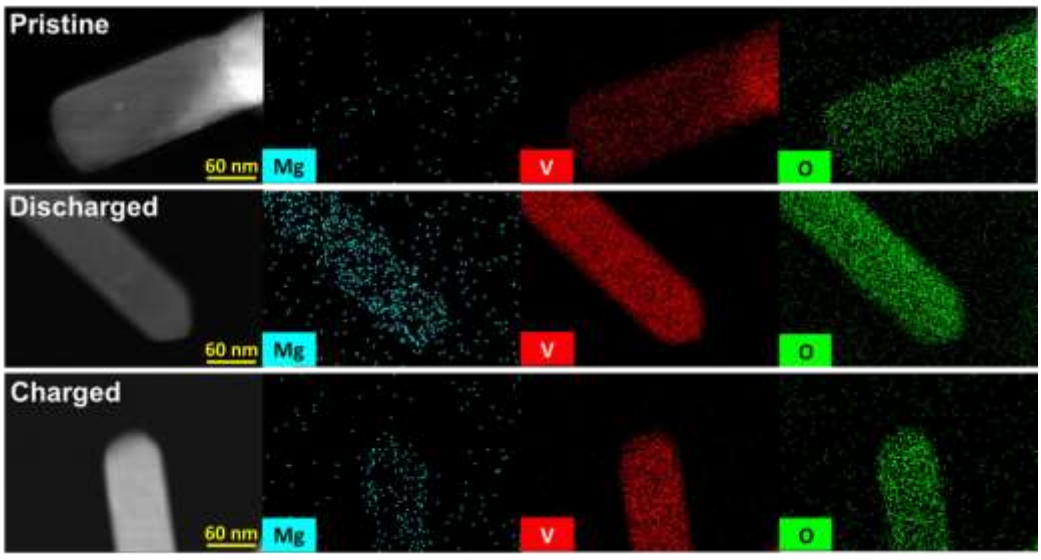

Figure 25. TEM-EDX of pristine, discharge, and charge electrode

XPS analysis results (Fig. 26) provide magnesium distribution evidence. The formation of the Mg 1s peak appeared in binding energy of 1304.4 eV during the discharge and disappeared after the charge state, demonstrate the successful magnesium intercalation into VO_2(B). Moreover, the V 2p spin-orbital spectra also observed in V^{4+} $2p_{1/2}$, V^{4+} $2p_{3/2}$ and V^{3+} $2p_{3/2}$ at 524.1, 516.7, and 515.8 eV, respectively. The V^{3+} $2p_{1/2}$ started to appear at lower binding energy during the discharge process and disappear as the original state at the charge, and in good agreement as reported previously.[30]

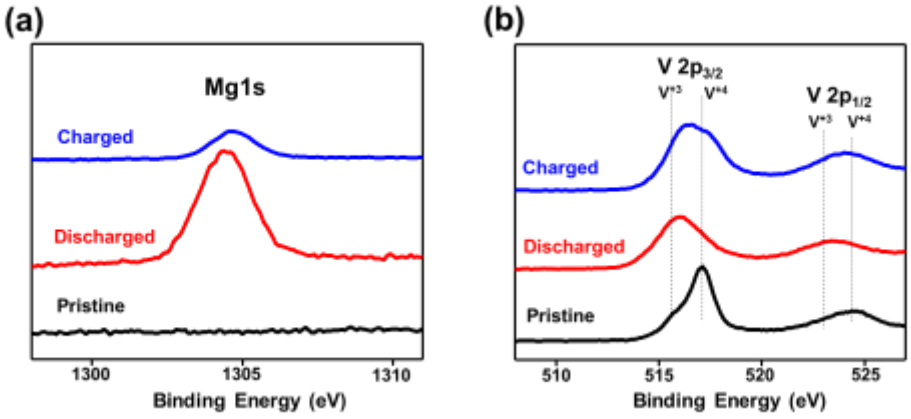

Figure 26. XPS analysis results (a) Mg1s. (b) V2p

IV. CONCLUSION

VO_2(B) has been synthesized using hydrothermal method and the structure of the material has been studied. The magnesium intercalation into the material also has been investigated in nonaqueous electrolyte. The material shows reversible magnesium ion intercalation in a nonaqueous electrolyte with a discharge capacity of 51 mAh g^{-1} at current density of 20 mA g^{-1} at room temperature. It also exhibits a discharge capacity of 114.8 mAh g^{-1} at a same current density, and an average voltage of ~2.47 V vs Mg/Mg^{2+} at 60^{o}C. The diffusion-controlled and surface-limited reaction was revealed using CVs, the intercalation was dominated ~80 % at 0.1 mVs^{-1}. The electrochemical analysis results provide feasibility of VO_2(B) to become MIBs cathode material.

The magnesium ion intercalation mechanism has been analyzed. The magnesium ion intercalation causes *(110)* plane enlarges. The more magnesium ion intercalation may cause irreversibility at the first cycle and further structural degradation. The magnesium ion position has been determined for the first time. Magnesium ions occupy the largest cavity of VO_2(B).

The results clearly provide magnesium intercalation mechanism into VO_2(B) in nonaqueous electrolyte and open up possibilities to discover new oxide cathodes with high performance for MIBs.

REFERENCES

[1] Noorden, R. V., “A better battery.” *Nature*, 507, 2014, pp. 26-28.

[2] Tackeray, M. M., Wolverton, C., and Isaac, E. D. “Electrical energy storage for transportation-approaching the limit of, and going beyond, lithium-ion batteries.” *Energy Environ. Sci*., 5, 2012, pp. 7854-7863.

[3] Tarascon, J. -M., and Armand, M. “Issues and challenges facing rechargeable lithium batteries.” *Nature*, 414, 2001, pp. 359–367.

[4] Nykvist, B., and Nilsson, “M. Rapidly falling costs of battery packs for electric vehicles.” *Nat. Clim. Change*, 5, 2015, pp. 329−332.

[5] Andre, D., Kim, S.-J., Lamp, P., Lux, S. F., Maglia, F., Paschos, O., and Stiaszny, B. “Future generations of cathode materials: an automotive industry perspective.” *J. Mater. Chem. A*, 3, 2015, pp. 6709− 6732.

[6] Grey, C. P., and Tarascon, J. M. “Sustainability and in situ monitoring in battery development.” *Nat. Mater*, 16, 2016, pp. 45−56.

[7] Canepa, P., Gautam, G. S., Hannah, D. C., Malik, R., Liu, M., Gallagher, K. G., Persson, K. A., and Ceder, G. “Odyssey of multivalent cathode materials: open questions and future challenges.” *Chem. Rev*, 117, 2017, pp. 4287−4341.

[8] Mohtadi, R., and Mizuno F. “Magnesium batteries: Current state of the art, issues and future perspectives.” *Beilstein J. Nanotechnol*, 5, 2014, pp. 1291–1311.

[9] Xu, C., Li, B., Du, H., and Kang, F. “Energetic zinc ion chemistry: The rechargeable zinc ion battery.” *Angew. Chem., Int. Ed*. 51, 2012, pp. 933−935.

[10] Ponrouch, A., Frontera, C., Barde, F., and Palacin, M. R. “Toward a calcium-based rechargeable battery.” *Nat. Mater*, 15, 2015, pp. 169-173.

[11] Aurbach, D., Lu, Z., Schechter, A., Gofer, Y., Gizbar, H., Turgeman, R., Cohen, Y., Moshkovich, M., and Levi, E. “Prototype systems for rechargeable magnesium batteries.” *Nature*, 407, 2000, pp. 724−727.

[12] Levi, E., Mitelman, A., Aurbach, D., and Brunelli, M. “Structural mechanism of the phase transitions in the Mg-Cu-Mo_6S_8 system probed by ex situ synchrotron X-ray diffraction.” *Chem. Mater*, 19, 2007, pp. 5131−5142.

[13] Levi, E., Gershinsky, G., Aurbach, D., Isnard, O., and Ceder, G. “New insight on the unusually high ionic mobility in chevrel phases.” *Chem. Mater*, 21, 2009. Pp. 1390−1399.

[14] Kaewmaraya, T., Ramzan, M., Osorio-Guillén, J., and Ahuja, R. “Electronic structure and ionic diffusion of green battery cathode material: $Mg_2Mo_6S_8$.” *Solid State Ionics*, 261, 2014, pp. 17−20.

[15] Chae, M. S., Heo, J. W., Lim, S.-C., and Hong, S.-T. “Electrochemical zinc-ion intercalation properties and crystal structures of $ZnMo_6S_8$ and $Zn_2Mo_6S_8$ chevrel phases in aqueous electrolytes.” *Inorg. Chem*, 55, 2016, pp. 3294−3301.

[16] Kai, K., Kobayashi, Y., Yamada, Y., Miyazaki, K., Abe, T., Uchimoto, Y., and Kageyama, H. “Electrochemical characterization of single-layer MnO_2 nanosheets as a high-capacitance pseudocapacitor electrode.” *J. Mater. Chem*, 22, 2012, pp. 14691−14695.

[17] Kaveevivitchai, W., and Jacobson, A. J. “High capacity rechargeable magnesium-ion batteries based on a microporous molybdenum vanadium oxide cathode.” *Chem. Mater*, 28, 2016, pp. 4593−4601.

[18] Sai Gautam, G., Canepa, P., Abdellahi, A., Urban, A., Malik, R., and Ceder, G. “The intercalation phase diagram of Mg in V_2O_5 from firstprinciples.” *Chem. Mater*, 27, 2015, pp. 3733−3742.

[19] Sa, N., Kinnibrugh, T. L., Wang, H., Gautam, G. S., Chapman, K. W., Vaughey, J. T., Key, B., Fister, T. T., Freeland, J. W., Proffit, D. L., Chupas, P. J., Ceder, G., Bareno, J. G., Bloom,

I. D., and Burrell, A. K. “Structural evolution of reversible Mg insertion into a bilayer structure of $V_2O_5 \cdot nH_2O$ xerogel material.” *Chem. Mater*, 28, 2016, pp. 2962−2969

[20] Makino, K., Katayama, Y., Miura, T., and Kishi, T. “Electrochemical insertion of magnesium to $Mg_{0.5}Ti_2(PO_4)_3$.” *J. Power Sources*, 99, 2001, pp. 66−69.

[21] Huang, Z.-D., Masese, T., Orikasa, Y., Mori, T., Minato, T., Tassel, C., Kobayashi, Y., Kageyama, H., and Uchimoto, Y. “$MgFePO_4F$ as a feasible cathode material for magnesium batteries.” *J. Mater. Chem. A*, 2, 2014, pp. 11578−11582.

[22] Zhang, R., and Ling, C. “Unveil the Chemistry of Olivine $FePO_4$ as magnesium battery cathode.” *ACS Appl. Mater. Interfaces*, 8, 2016, pp. 18018−18026.

[23] Wu, J., Gao, G., Wu, G., Liu, B., Yang, H., Zhou, X., and Wang, J. “Tavorite-$FeSO_4F$ as a potential cathode material for Mg ion batteries: a first principles calculation.” *Phys. Chem. Chem. Phys*, 16, 2014, pp. 22974− 22978.

[24] Kim, D.-M., Kim, Y., Arumugam, D., Woo, S. W., Jo, Y. N., Park, M.-S., Kim, Y.-J., Choi, N.-S., and Lee, K. T., “Co-intercalation of Mg^{2+} and Na^+ in $Na_{0.69}Fe_2(CN)_6$ as a high-voltage cathode for magnesium batteries.” *ACS Appl. Mater. Interfaces*, 8, 2016, pp. 8554−8560.

[25] Kulish, V. V., and Manzhos, S. “Comparison of Li, Na, Mg, and Al-ion insertion in vanadium pentoxides and vanadium dioxides.” *RSC Adv*, 7, 2017, pp. 18643-18649.

[26] Mai, L., Wei, Q., An, Q., Tian, X., Zhao, Y., Xu, X., Xu, L., Chang, L., and Zhang, Q. “Nanoscroll buffered hybrid nanostructural VO_2 (B) cathodes for high rate and long life lithium storage.” *Adv. Mater*, 25, 2013, pp. 2969–2973.

[27] Wang, W., Jiang, B., Hu, L., Lin, Z., Hou, J., and Jiao, S. “Single crystalline VO_2 nanosheet : a cathode material for sodium batteries with high rate cycle performance.” *Journal of Power Sources*, 250, 2014, pp. 181-187.

[28] Liu, P., Xu, Y., Zhu, K., Bian, K., Wang, J., Sun, X., Gao, Y., Luo, H., Lu, L., and Liu, J. “Ultrathin VO_2 nanosheet self-assembled into 3D micro/nano-structured hierarchical porous

sponge-like micro-bundles for long-life and high-rate Li-ion batteries." *J. Mater. Chem. A*, *5*, 2017, pp. 8135–8772.

[29] Niu, C., Meng, J., Han, C., Zhao, K., Yan, M. and Mai, L. "VO_2 nanowires assembled into hollow microspheres for high-Rate and long-life lithium batteries". *Nano Lett*, 14, 2014, pp. 2873−2878.

[30] Pei, C., Xiong, F., Sheng, J., Yin, Y., Tan, S., Wang, D., Han, C., An, Q., and Mai, L. "VO_2 nanoflakes as the cathode material of hybrid magnesium-lithium-ion batteries with high energy density." *ACS Appl. Mater. Interfaces*, 9, 2017, pp. 17060−17066.

[31] Ding, J., Du, Z., Gu, L., Li, B., Wang, L., Wang, S., Gong, Y., and Yang, S. "Ultrafast Zn^{2+} intercalation and deintercalation in vanadium dioxide." *Adv. Mater*, 30, 2018, pp. 1800762.

[32] Mahadi, N. B., Park, J-S., Park, J-H., Chung, K-Y., Yi, S. Y., Sun, Y-K., and Myung, S-T. "Vanadium dioxide-reduced graphene oxide composite as cathode materials for rechargeable Li and Na batteries." *Journal of Power Sources*, 326, 2016, pp. 522-532.

[33] Xia, C., Lin, Z., Zhou, Y., Zhao, C., Liang, H. Rozier, P., Wang, Z., and Alshareef, H. N. "Large intercalation pseudocapacitance in 2D VO_2 (B): breaking through the kinetic barrier." *Adv. Mater*, 30, 2018, pp. 1803594.

[34] Li, H., He, P., Wang, Y., Hosono, E., and Zhou, H. "High-Surface vanadium oxides with large capacities for lithium-ion batteries: from hydrated aerogel to nanocrystalline VO_2(B), V_6O_{13} and V_2O_5." *J. Mater. Chem*, 21, 2011, pp. 10999−11009.

[35] Chao, D., Zhu, C., Xia, X., Liu, J., Zhang, X., Wang, J., Liang, P., Lin, J., Zhang, H., Shen, Z. X., and Fan, H. J. "Graphene quantum dots coated VO_2 arrays for highly durable electrodes for Li and Na ion batteries." *Nano Lett*, 15, 2015, pp. 565−573.

[36] Ren, G., Hoque, M. N. F., Pan, X., Warzywoda, J., and Fan, Z. "Vertically aligned VO_2(B) nanobelt forest and its three-dimensional structure on oriented graphene for energy storage." *J. Mater. Chem. A*, 3, 2015, pp. 10787−10794.

[37] Luo, T., Liu, Y., Su, H., Xiao, R., Huang, L., Xiang, Q., Zhou, Y., and Chen, C. "Nanotructured VO_2 (B) : A high capacity magnesium-ion cathode and its electrochemical reaction mechanism." *Electrochimica Acta*, 260, 2018, pp. 805-813.

[38] Liu, Q., Tanc, G., Wanga, P., Abeyweerad, S. C., Zhangd, D., Rongb, Y., Wua, Y. A., Luc, J., Sunb, C-J., Renb, Y., Liua, Y., Muehleisene, R. T., Guzowskie, L. B., Lif, J., Xiaob, X., and Sund, Y. "Revealing mechanism responsible for structural reversibility of singlecrystal VO_2 nanorods upon lithiation/delithiation." *Nano Energy*, 36, 2017, pp. 197–205.

[39] Li, S., Liu, J-. B., Wan, Q., Xu, J., and Liu, B-. X. "First-Principles analysis of Li intercalation in VO_2(B)." *Chem. Mater*, 29, 2017, pp. 10075−10087.

[40] Koch D., Kulish, V. V., and Manzhos, S. "A first-principles study of potassium insertion in crystalline vanadium oxide phases as possible potassium-ion battery cathode materials." *MRS Communications*, 7, 2017, pp. 819–825.

[41] Popuria, S. R., Artemenkoa, A., Labrugered, C., Miclauc, M., Villesuzannea, A., and Pollet, M. "VO_2 (A): Reinvestigation of crystal structure, phase transition and crystal growth mechanisms." *Journal of Solid State Chemistry*, 213, 2014, pp. 79–86.

[42] Yao, T., Oka, Y., and Yamamoto, N. "A structural study of the high temperature phase of VO_2(A)." Journal of Solid State Chemistry, 112, 1994, pp. 196-198.

[43] Zhang, W., Shi, L., Tang, K., and Yu1, Y. "A facile fabrication of VO_2(A) micro-nanostructures with controlled shape and its electrochemical behavior in lithium ion batteries." *Chem. Lett.*, 2012, 41, pp. 104-106.

[44] Dai, L., Gao, Y., Cao, C., Chen, Z., Luo, H., Kanehira, M., Jin, J., and Liu, Y. "VO_2 (A) nanostructures with controllable feature sizes and giant aspect ratios: one-step hydrothermal synthesis and lithium-ion battery performance." *RSC Advances*, 2, 2012, pp. 5265–5270.

[45] Hu, X., Zhao, Z., Wang, L., Li, J., Wang, J., Zhao, Y., and Jin, H. "VO_2(A)/graphene nanostructure : stand up to Na ion intercalation/deintercalation for enhanced electrochemical performance as a Na-ion battery cathode." Electrochimica Acta, 293, 2019, pp. 97-104.

[46] Toby, B. H.” EXPGUI, a graphical user interface for GSAS.” *J. Appl. Crystallogr*, 34, 2001, pp. 210−213.

[47] Betteridge, P. W., Carruthers, J. R., Cooper, R. I., Prout, K., and Watkin, D. J. “CRYSTALS version 12: software for guided crystal structure analysis.” *J. Appl. Crystallogr*, 36, 2003, pp. 1487−1487.

[48] Lee, E., and Hong, S.-T. “Sr_4AlNbO_8: A new crystal structure type determined from powder X-ray data.” *J. Solid State Chem*, 181, 2008, pp. 2930−2934.

[49] Rohlicek, J., and Husak, M. “MCE2005 - a new version of a program for fast interactive visualization of electron and similar density maps optimized for small molecules.” *J. Appl. Crystallogr*, 40, 2007, pp. 600−601.

[49] Wang, J., Polleux, J., Lim, J., and Dunn, B. “Pseudocapacitive contributions to electrochemical energy storage in TiO_2 (anatase) nanoparticles.” *J. Phys. Chem. C*, 111, 2007, pp. 14925−14931.

[50] Deylami, M. R-., Chae, M. S., and Hong, S. T. “$H_2V_3O_8$ as a high energy cathode material for nonaqueous magnesium-ion batteries.” *Chem. Mater*, 30, 2018, pp. 7464-7472.

[51] Lim, S. C., Lee, J., Kwak, H. H., Heo, J. W., Chae, M. S., Ahn, D., Jang, Y. H., Lee, H., and Hong, S. T. “Unraveling the magnesium-ion intercalation mechanism in vanadium pentoxide in a wet organic electrolyte by structural determination.” *Inorg. Chem*, 56, 2017, pp. 7668−7678.

요 약 문

이산화바나듐으로의 마그네슘 이온 삽입의 구조 및 전기 화학적 특성

리튬 이온 배터리 (LIB)와 같은 에너지 저장 기술은 모바일, 랩탑, 전기 자동차 및 에너지 저장 시스템을 비롯한 유비쿼터스 휴대용 전자 장치의 개발을 가능하게했다. 1991 년 소니가 최초로 고전압 및 고에너지 셀을 상용화 한 이후, 현대의 LIB 는 중량당 에너지밀도가 지금까지 두 배 이상 증가하면서 놀라운 가능성을 제시하였다. 그럼에도 불구하고 세계적으로 국지적인 리튬의 분포, 셀 엔지니어링 및 처리 비용에 대한 문제는 여전히 많은 연구자들이 해결해야 할 과제들 중 하나이다. 차세대 LIB 기술의 한 유형으로서, 다가 이온 배터리 (Mg^{2+}, Ca^{2+} 및 Zn^{2+} 등)는 위와 같은 문제에 대한 기준을 충족시키는 특성을 갖는 것으로 간주된다. 다가 이온 배터리 양극재료에 대한 연구는 새로운 재료 및 전기화학적 층간삽입화학에 대한 발견을 제공한다. 그러나, 층간삽입과정은 격자구조에서 양이온과 산소 이온 사이의 강한 Coloumbic 상호작용으로 인해 산화물 내에서 느리게 발생할 수 있다. 결과적으로, 다가 이온의 양극물질로의 전기 화학적 층간삽입화학은 여전히 기능성 물질의 발견 가능성 뿐만 아니라 밝혀지지 않은 수수께끼 같은 현상이 공존하는 것으로 간주된다.

마그네슘 이온 배터리 (MIBs)는 마그네슘이 지구상에서 풍부하기 때문에 유망하다고 할 수 있으며 높은 에너지 밀도, 안전성 및 경제적인 에너지 저장을 제공할 수 있다. 그러나, 지금까지 MIBs 양극물질에 대해서 제한된 후보물질 만이 제시되었다. 이 연구에서는, 이산화바나듐 (VO_2(B))으로 마그네슘 이온이 삽입된 구조 및 전기화학적 특성이 밝혀졌다. 이산화바나듐 다형체는 VO_2(B), VO_2(A), VO_2(M), VO_2(R) 및 VO_2(C)의 여러 결정상으로 존재하며, 여기서 VO_2(B) 및 VO_2(A)는 준안정상으로 간주된다. VO_2(B)는 물질의 가장 안정적인 개방형 구조로 간주되는 브루카이트 이산화바나듐 상이다. VO_2(B)의 결정 구조는 *C2/m* 의 공간 그룹을 갖는 단사정계 구조를 가지며 VO_6 팔면체 사이의 모서리 공유에 의해 형성되고, C1, C2 및 C3 으로 표시 된 3 개의 확산 공동 및 b 축과 c 축을 따라 2 개의 확산 경로를 제공한다.

VO_2(B)는 용이한 열수법을 사용하여 합성되었고, 공간 그룹 *C2/m*, 및 나노-벨트 형태를 갖는 단사정계 구조가 XRD, HR FE-SEM 및 TEM 에 의해 확인되었다. VO_2(B)는 a = 12.059 (1) Å, b = 3.692 (2) Å, c = 6.420 (1) Å 의 격자상수를 갖는다. 불순물이 발생하지 않았으며, 이는 합성공정동안 V^{5+}가 V^{4+}로 성공적으로 환원되었음을 의미한다.

건식전해질에서 AC 에 대해 -0.57V 에서 더 급격한 감소 피크를 나타내는 0.1mV s^{-1} 의 스캔 속도를 갖는 습식전해질에서의 VO_2(B)의 CV 프로파일. 한편 건식 전해질의 산화 피크는 습식 전해질 (0.18V vs AC)보다 높은 전압 (0.35V vs AC)에서 나타난다. VO_2(B)는 비수계전해질 (51 mAh g^{-1})에 비해 습식전해질에서 250mAh g^{-1} 의 훨씬 큰 방전 및 충전 용량을 나타냈다. 이 물질은 건식전해질 (0.5 M $Mg(ClO_4)_2$ in AN)에서 20mA g^{-1} 의 전류 밀도에서 25°C 에서 방전 용량이 51.0 mAh g^{-1} 의 가역적인 마그네슘 층간삽입을 보여준다. 25, 30, 40 및 50 mA g^{-1} 에서 우수한 율속특성을 보여줍니다. VO_2(B)의 사이클 성능은 전해질에서의 구조적 분해 및

바나듐 용해로 인해 25 사이클 후 초기 용량의 62 %에 도달하여 여전히 개선이 필요하다. 환원 및 산화 반응은 층간 메카니즘에 의해 지배되며, 약 81-75 %의 마그네슘 이온이 0.1 mV s^{-1} 의 주사속도로 삽입된다. 주사속도가 1 mV s^{-1} 로 증가함에 따라 표면제한메커니즘은 천천히 증가합니다.

VO_2(B)는 또한 건식 전해질에서 60°C 에서 ~ 2.47 V (vs Mg/Mg^{2+})의 평균 전압으로 114.8mAh g-1 의 방전 용량으로 마그네슘 층간삽입을 나타낸다. 선명한, 방전 및 충전 상태에서 마그네슘 이온 intercalation 에 의한 VO_2(B) 구조적 변화를 공개한다. $Mg_{0.11}VO_2$ 의 결정 구조와 VO_2(B)의 세부 마그네슘 이온 위치가 처음으로 밝혀졌다. 그것은 공간 그룹 *C2/m* 의 단 사정 구조를 가지고 있으며 마그네슘 이온은 VO_2(B)의 가장 큰 공동에 위치합니다. TEM-EDX 매핑 및 XPS 결과는 구조적으로 가역적인 마그네슘 층간삽입이 일어났음을 보여주었다. 방전된 전극에서 균일 한 분포를 명확하게 볼 수 있으며, 충전 전극에서는 다시 사라지는 가역 반응이 일어난다. Mg 1s 피크의 형성은 방전 동안 1304.4 eV 의 결합 에너지에서 관측되고 충전 후에 사라졌으며, 이는 VO_2(B) 로의 성공적인 마그네슘 삽입을 보여준다. 결과적으로 건식 전해질에서 VO_2(B)로 마그네슘 층간삽입 메커니즘이 명확하게 드러나며 MIBs 에 대해 고성능의 새로운 산화물 양극재를 발견 할 수 있는 가능성을 열어준다.

ACKNOWLEDGEMENT

Firstly, all prises belong to Almighty God who gives us life, strength, and time as well as opportunity to finish this master's thesis. Secondly, I would thank to my supervisor, Prof. Seung-Tae Hong, co-advisor, Prof. Hochun Lee, and the committee member, Prof. Yong Min Lee for the great guidance so far. I want to thank my parents, brother, and little sisters, and also Sukma for all the motivations and emotional supports whenever I needed. A huge respect and appreciation go for my great labmate, Munseok Chae, who contribute a lot to my works. I also want to thank all Discovery Lab members, Boosik hyung, Hyojeong nuna, Jeyne hyung, my friend Hyeri and Dongmin, and Jiyoung and also alumnae, Jongwook hyung, Jooeun nuna, and Hunho hyung. A great appreciation also goes to all my Indonesian family in DGIST, Mbak Elok, Humaira, Kak Indra, Kang Syamsul, Mbak Ana, Kang Iman, Mbak Dina, Kak Tyo, and Kak Reisa for the companion. Lastly, all thanks to my Korean and Foreigner friends who I can not mention all the names. More success will come.